A Multimodel Assessment of RKW Theory's Relevance to Squall-Line Characteristics

GEORGE H. BRYAN AND JASON C. KNIEVEL

National Center for Atmospheric Research, Boulder, Colorado*

MATTHEW D. PARKER

Department of Marine, Earth, and Atmospheric Sciences, North Carolina State University, Raleigh, North Carolina

(Manuscript received 7 September 2005, in final form 20 December 2005)

ABSTRACT

The authors evaluate whether the structure and intensity of simulated squall lines can be explained by "RKW theory," which most specifically addresses how density currents evolve in sheared environments. In contrast to earlier studies, this study compares output from four numerical models, rather than from just one. All of the authors' simulations support the qualitative application of RKW theory, whereby squall-line structure is primarily governed by two effects: the intensity of the squall line's surface-based cold pool, and the low- to midlevel environmental vertical wind shear. The simulations using newly developed models generally support the theory's quantitative application, whereby an optimal state for system structure also optimizes system intensity. However, there are significant systematic differences between the newer numerical models and the older model that was originally used to develop RKW theory. Two systematic differences are analyzed in detail, and causes for these differences are proposed.

1. Introduction

Many studies of numerically simulated squall lines implicate the surface-based cold pool and environmental vertical wind shear as critical factors in determining a system's structure and evolution (e.g., Hane 1973; Thorpe et al. 1982; Nicholls et al. 1988; Fovell and Ogura 1989; Szeto and Cho 1994; Fovell and Dailey 1995; Robe and Emanuel 2001; Parker and Johnson 2004a; James et al. 2005). An ongoing area of research addresses *why* details such as cold pool intensity and shear are important. To this end, in 1988 Rotunno et al. (1988; hereafter referred to as RKW88) and Weisman et al. (1988, hereafter referred to as WKR88) advanced a theory based on numerical simulations, theoretical reasoning, and an observational review. Their theory—now often called "RKW theory" after the three authors' names—argues that environmental shear "fundamentally alters" the circulation associated with a density current (i.e., cold pool). Specifically, the shear counteracts the cold pool's tendency to sweep environmental air over the top of the cold pool. An optimal state exists wherein the shear approximately balances the cold pool's circulation, leading to the deepest lifting of environmental air.

Extending the theory to more complex squall lines, RKW88 argued that lifting at the leading edge of cold pools is an essential element in squall lines, because it generates new convective cells. Thus, RKW88 concluded that the combination of the relative effects of cold pool intensity and environmental shear is also an important mechanism for squall-line strength and evolution. The applicability of RKW theory to squall lines, rather than just to density currents in isolation, was addressed in a broad series of numerical simulations by RKW88 and WKR88. The authors concluded that the relative balance of cold pool intensity and shear magnitude was the "most significant factor" in determining squall-line structure, evolution, and intensity.

These conclusions were reassessed recently by Weisman and Rotunno (2004, hereafter referred to as WR04). Their study had two parts. In the first, their

* The National Center for Atmospheric Research is sponsored by the National Science Foundation.

Corresponding author address: George H. Bryan, National Center for Atmospheric Research, 3450 Mitchell Lane, Boulder, CO 80301.
E-mail: gbryan@ucar.edu

idealized simulations of cold pools spreading in sheared flow reconfirmed the main element of RKW theory (i.e., that "cold-pool lifting is especially enhanced by low-level shear"; WR04, p. 363). Their simulations demonstrated that deepest lifting occurs when the two processes (cold pool and shear) approximately balance, and when shear is confined to the cold pool depth. The authors also addressed a series of papers that investigated this problem from a different perspective (e.g., Xu et al. 1996; Xue et al. 1997; Xue 2000a, 2002), as summarized in the first paragraph in section 2 of the paper by WR04.

In the second part of their paper, WR04 evaluated the degree to which RKW theory's cold pool–shear interaction could explain the structure, evolution, and intensity of simulated squall lines in a broad range of environmental shears, including deep layers of shear and elevated layers of shear. The authors also used larger domains and higher resolution than were used by WKR88, and they used more quantitative measures of system intensity in their analysis. WR04 concluded that their results reconfirmed the findings of RKW88 and WKR88 that the relative effects of the cold pool and shear can explain many aspects of squall-line structure and intensity. However, WR04 concluded (p. 380) that one aspect of their earlier studies—system longevity—can no longer be considered a part of their argument, because all of their simulated squall lines were long lived (out to 6 h). The cause of the rapid squall-line demise in the simulations by RKW88 and WKR88 was first explained by Fovell and Ogura (1989, their section 5a).

From a certain perspective, *RKW theory is not a theory for strong, long-lived squall lines*, despite the titles chosen by RKW88 and WR04. Most specifically, the theory addresses and explains the interaction between density currents and environmental shear. Many meteorologists, however, are interested in how well RKW theory applies to squall-line characteristics, such as structure and intensity.

As applied to squall-line structure, RKW theory's relevance is summarized in conceptual figures such as WR04's Fig. 2. That is, systems lean upshear when the cold pool is more intense than the low- to midlevel shear, and systems lean downshear when the shear is more intense than the cold pool. The optimal state is the condition wherein these two effects roughly balance, and the system's updrafts are approximately upright and collocated with the surface gust front (i.e., the leading edge of the cold pool). Therefore, as discussed by WR04 (p. 381), the optimal state for squall-line structure is simply one point in a continuum, with outflow-dominated systems on one end, and shear-dominated systems on the other end. The ability of suboptimal squall lines (from the perspective of RKW theory) to be strong and long lived has been pointed out by many authors since RKW88, including (but not limited to) WKR88, Fovell and Ogura (1988, 1989), Lafore and Moncrieff (1989), Rotunno et al. (1990), and Coniglio and Stensrud (2001). There is also some debate about the exact structure of a squall line in the optimal state, with notable conceptual models being offered by Fovell and Ogura (1989, their "solitary, persistent updraft") and by James et al. (2005, their "slabular convective line").

As applied to squall-line intensity, RKW theory's relevance is not immediately obvious, because the intensity of lifting at the cold pool edge is not necessarily related to overall system intensity. Therefore, a primary goal of the squall-line simulations by WR04 was to address this application of the theory. WR04 showed that some measures of system intensity (e.g., total rainfall and surface wind speed) were enhanced in a manner that was consistent with RKW theory's focus on the relative effects of cold pools and shear.

Stensrud et al. (2005) recently questioned whether the relative strengths of cold pools and shear have any relevance to squall-line structure and intensity, particularly in observed systems. They had several specific concerns. Of particular interest to us, Stensrud et al. noted that some quantitative measures of system intensity in WR04's results were not largest for systems that were near the optimal state from the perspective of RKW theory. The authors contended that if the intensity of cold pool lifting is directly relevant to squall-line intensity, there should be a peak in system intensity approximately near the optimal state.

However, we question whether this lack of an expected peak in system intensity in WR04's results is a general weakness of RKW theory's applicability to squall-line intensity, or whether it is an artifact of the numerical model used by WR04. That different models produce different results is widely recognized in mesoscale research, and many studies have addressed the issue. For instance, several model comparisons have recently been conducted on deep precipitating convection (e.g., Moncrieff et al. 1997; Richardson 1999; Redelsperger et al. 2000; Xu et al. 2002; Derbyshire et al. 2004). Some of these studies used as few as two models, while others used up to eight. One of the main goals of these and other such studies is to identify large differences in the output among different numerical models. By doing so, a model comparison can call attention to specific model components that influence sensitivity, which then guides future model development and aids interpretation of output by model users.

TABLE 1. Summary of the numerical model configurations. The information under "Advection" and "Diffusion" refers to the order of the truncation error of the numerical scheme (when specified as second, third, etc.), or to some other detail of the formulation. The schemes are separated by their formulation in the horizontal and vertical.

Model	Advection (horizontal/vertical)	Diffusion (horizontal/vertical)	Other details
Comparison members:			
KW	Fourth/second	Fourth/second	
ARPS-A	Fourth/fourth	Fourth/none	
ARPS-B	Fourth/fourth	Fourth/none (u, v, w only)	Scalar advection is FCT/FCT
WRF-A	Fifth/third	Implicit, flow dependent	$C_k = 0.10$
WRF-B	Fifth/third	Implicit, flow dependent	$C_k = 0.15$
BF-A	Fifth/fifth	Implicit, flow dependent	
BF-B	Fifth/fifth	Implicit, flow dependent	Scalar advection is WENO/WENO
Special simulations:			
BF-C	Fifth/fifth	Implicit, flow dependent	BF-A, but without water conservation
BF-D	Fifth/fifth	Implicit, flow dependent	BF-C, but with KW vertical diffusion

As an example, Redelsperger et al. (2000) analyzed results from idealized simulations of a tropical squall line using eight numerical models. The authors found excellent qualitative agreement among models in terms of overall system structure and evolution. In contrast, some quantitative results such as rainfall rate differed greatly (by more than a factor of 3). Redelsperger et al. identified three model details that were most responsible for differences among their simulations: the microphysics parameterization, the use of two dimensions (i.e., x–z) compared to three, and the lateral boundary conditions. They recommended that further research should focus on improving these aspects of numerical model configurations.

As far as we know, there has been no systematic evaluation of RKW theory's relevance to squall-line properties that is based on a model other than that used by RKW88 and WR04. Therefore, the main goal of our study is to assess whether RKW theory's relevance to squall lines is supported by other numerical models.

We base our new simulations on the recent study by WR04, using the same simulation details and analysis techniques. We use three additional numerical models, all of which have been developed more recently than the model used by WR04. Our findings provide guidance for interpreting previously published results, and have implications for ongoing model development.

2. Methodology

a. Numerical models

We present results from four numerical models in this study. All are compressible models that use time splitting to account for the acoustic modes (e.g., Klemp and Wilhelmson 1978; Skamarock and Klemp 1994). All models use the staggered C grid (Arakawa and Lamb 1977), and all simulations use the same physical parameterizations, including the Kessler (1969) liquid-only microphysics scheme and the Deardorff (1980) turbulence parameterization based on a prognostic equation for turbulence kinetic energy. For three of the models, two different model configurations are used in order to highlight how well the models agree with themselves in addition to how well they agree with one another. Thus, there are seven output members, as summarized in Table 1.

One of the members is the Klemp–Wilhelmson (KW) model. The KW model uses leapfrog-in-time integration with fourth-order derivatives for horizontal advection and second-order derivatives for vertical advection (Klemp and Wilhelmson 1978; Wilhelmson and Chen 1982). To remove small-scale numerical noise, fourth-order artificial diffusion is used in the horizontal and second-order vertical diffusion acting on perturbation fields is used in the vertical. For this study, we utilize the results from the KW model reported by WR04.

The second numerical model is version 4.5.2 of the Advanced Regional Prediction System (ARPS) model (Xue et al. 2000). This model also uses leapfrog-in-time integration. For one configuration, referred to as ARPS-A, the model setup is similar to that for the KW model. Fourth-order advection is used in all directions. Fourth-order diffusion is applied in the horizontal only. The diffusion coefficient is the default value for ARPS 4.5.2, which is roughly one-half of that used by WR04. We ran additional simulations with different diffusion coefficients and they had no influence on the main conclusions of this paper; therefore, we present only simulations using the default diffusion coefficient. A newer version of the ARPS model has a monotonic limiter available for high-order diffusion (Xue 2000b); this scheme was not used herein, but Bryan (2005, p. 1993)

found it to have little impact on simulations using fourth-order diffusion. There is no artificial vertical diffusion in the ARPS-A simulations. For the second configuration, ARPS-B, the advection of scalars is calculated by a Flux Corrected Transport (FCT) scheme (Zalesak 1979) using a fourth-order term for the high-order flux. This configuration is preferred by many ARPS users (e.g., Xue 2000a, Xue 2002), particularly for its ability to prevent artificial negative water values (e.g., Xue et al. 2001). The artificial diffusion of scalars is turned off for this latter configuration. The ARPS model also has a positive definite advection scheme for moisture and turbulence kinetic energy [i.e., the multidimensional positive definite centered difference (MPDCD) scheme; Xue et al. 2001, p. 151], but we did not use this scheme. A high-resolution two-dimensional simulation of a squall line that addresses aspects of model design is presented in section 5 of Xue (2002).

The third numerical model is version 2.0.3.1 of the Advanced Research core of the Weather Research and Forecasting (WRF) model (Skamarock et al. 2005). This model utilizes a hydrostatic pressure vertical coordinate and is the only model analyzed herein that does not use Cartesian height as the vertical coordinate. This version of the WRF model uses third-order Runge–Kutta time integration (Wicker and Skamarock 2002). The advection formulation for these simulations is fifth order in the horizontal and third order in the vertical. These odd-ordered schemes are upwind biased and contain implicit diffusion that is proportional to the advective wind speed. No additional artificial diffusion term is used. The two WRF model configurations use different values for C_k, a parameter in the subgrid turbulence parameterization that is proportional to the amount of diffusion applied by this scheme (Takemi and Rotunno 2003). One configuration, WRF-A, uses a typical value, $C_k = 0.10$. The second configuration, WRF-B, uses $C_k = 0.15$, based on the recommendation of Takemi and Rotunno in their 2005 corrigendum (Takemi and Rotunno 2003).

The fourth numerical model is version 1.8 of the Bryan–Fritsch (BF) cloud model (Bryan and Fritsch 2002). This model uses the same third-order Runge–Kutta time integration technique as the WRF model uses. For these simulations, the governing equations are slightly different from those in the other models; these equations improve conservation of total mass and total energy compared to traditional cloud model equations (Bryan and Fritsch 2002). For one configuration, BF-A, the advection scheme is fifth order in all directions, with no artificial diffusion. For the other configuration, BF-B, the advection of scalars uses the weighted essentially nonoscillatory (WENO) scheme of Shu (2001).

In summary, there are six simulation members that use the relatively newly developed ARPS, WRF, and BF models. Three of the members are configured with comparatively low diffusion, and are denoted with "-A." The other three members, denoted with "-B," have either increased diffusion or use nonoscillatory advection schemes, which are typically more diffusive than standard, oscillatory schemes. The seventh member of the simulations is a single configuration of the KW model.

The diversity of the models in our study is rather narrow: all use finite differences on structured grids, all are compressible and use the same time-splitting integration technique, and all are configured to use the same liquid-only microphysics scheme (Kessler 1969; Klemp and Wilhelmson 1978). Thus, the scope of the conclusions from this model comparison is limited from the perspective of model development. Nonetheless, these models are commonly used to study severe storms, and a comparison of their strengths and weaknesses has merit.

b. Simulation design

The design of the numerical simulations is generally the same as that used by WR04. The resolution, physics schemes, and environmental conditions are constrained by the choices made by WR04, because our study addresses whether various numerical models support the conclusions of RKW88 and WR04.

One of the few ways in which our setup differs from that used by WR04 is the domain dimensions, which are 600 km $\times$ 80 km $\times$ 20 km. The slightly deeper domain (20 km as opposed to 17.5 km used by WR04) is necessary to accommodate a Rayleigh damper at the top of the domain in the new simulations; an open radiative condition was used by WR04. The smaller along-line dimension (80 km as opposed to 160 km used by WR04) reduces the cost of our simulations. Based on a limited set of simulations using the BF model, we find this smaller along-line length to be sufficient for the types of qualitative and quantitative conclusions addressed in this paper. As configured by WR04, the longer horizontal dimension is in the across-line direction, and open conditions are used at the boundaries. The shorter horizontal dimension is in the along-line direction, and periodic boundary conditions are used.

For all of our simulations, the squall lines are initiated with a 1.5-K perturbation in potential temperature (θ) at $x = 300$ km, as specified by WR04. A more intense perturbation was required to initiate squall lines with the KW model in some strong shear cases (WR04, p. 369). This was not necessary with the newer numerical models, with two exceptions. One is the ARPS-B

configuration with the strongest shear used herein, which eventually produces a squall line, but later than with all other model configurations. The second is the WRF-B configuration, also with the strongest shear, which does not produce a squall line at all. We decided to retain these simulations rather than redo them with a stronger perturbation, because one of our goals is to reveal any systematic differences that are inherent in certain model configurations. It is useful to document that these two more diffusive, -B, configurations require stronger forcing to initiate convection in some environments, as does the KW model.

In all other respects, the simulation details are the same as those described by WR04. Small-amplitude ($\leq$0.1 K) θ perturbations are inserted into the line thermal to initiate three-dimensional motion. The horizontal grid spacing is 1 km. All models use 40 vertical levels. For the height-coordinate models, this means the vertical grid spacing is constant at 500 m. For the WRF model, the vertical grid spacing at the initial time varies between 485 and 525 m. The initial thermodynamical environment is horizontally homogeneous, using the same analytic sounding as used by WR04 (Fig. 1). All simulations last 6 h.

In this study, we investigate only wind profiles with across-line shear in the 0–5-km layer. Specifically, linear shear is specified from 0 to 5 km, with a constant wind speed above 5 km. We refer to the simulations by the amount of wind variation in the 0–5-km layer (ΔU). The along-line wind is zero.

We focus exclusively on the 0–5-km layer because most of WR04's figures are from simulations with this shear profile. We do not have access to the output from their simulations, so we rely on the figures available in their paper. WR04 did find that systems were more intense when shear was confined to the lowest 2.5 km—the approximate depth of the cold pool—and that bow echoes were more prevalent in shallow shear. We stress that our study does not address all aspects of RKW theory and its applicability to squall lines, particularly because we focus on a narrow range of conditions. Nonetheless, we show in the next section that shear variations in the 0–5-km layer can produce a broad range of squall line structures, which is a key element of our model comparison.

3. System structure

Using the KW model, WKR88 and WR04 demonstrated that an impressively broad range of system structures could be created by changing only low- to midlevel shear perpendicular to the squall line. For example, in weak 0–5-km shear, simulated systems were

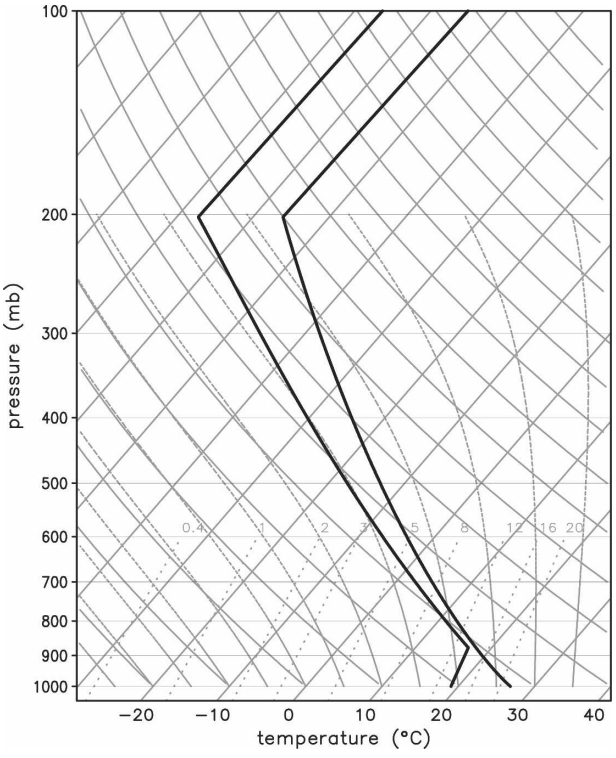

FIG. 1. The initial thermodynamical sounding.

tilted upshear and contained mainly weak, scattered updrafts. In moderate 0–5-km shear, simulated systems were nearly upright, and updrafts were more continuous along the line. In even stronger 0–5-km shear, systems were tilted downshear, with strong, isolated cells that sometimes had supercellular characteristics.

These qualitative results hold for all of our simulations using the newer models. That is, the trend from upshear-tilted to downshear-tilted systems with increasing 0–5-km shear occurs in all simulations (Figs. 2–4). In addition, individual updrafts tend to be weaker and smaller in the weakly sheared environments (Fig. 5), but stronger and larger in the strongly sheared environments (Fig. 6).

Among model simulations, differences in the overall system structure are minor. For example, when ΔU = 10 m s^{-1}, all models produce cold pools that are deepest within ~30 km of the surface gust front, and a cloud extends mostly upshear of the gust front (Fig. 2). When ΔU = 20 m s^{-1}, the cloud at upper levels is more symmetric, and the overall system structure is more upright (Fig. 3) than it is in weaker shear. When ΔU = 30 m s^{-1}, the cloud extends mostly downshear in every case (Fig. 4). For any value of ΔU, overall flow patterns are similar among all models.

One notable difference in our study is the tendency for the more diffusive, -B, simulations to have slightly

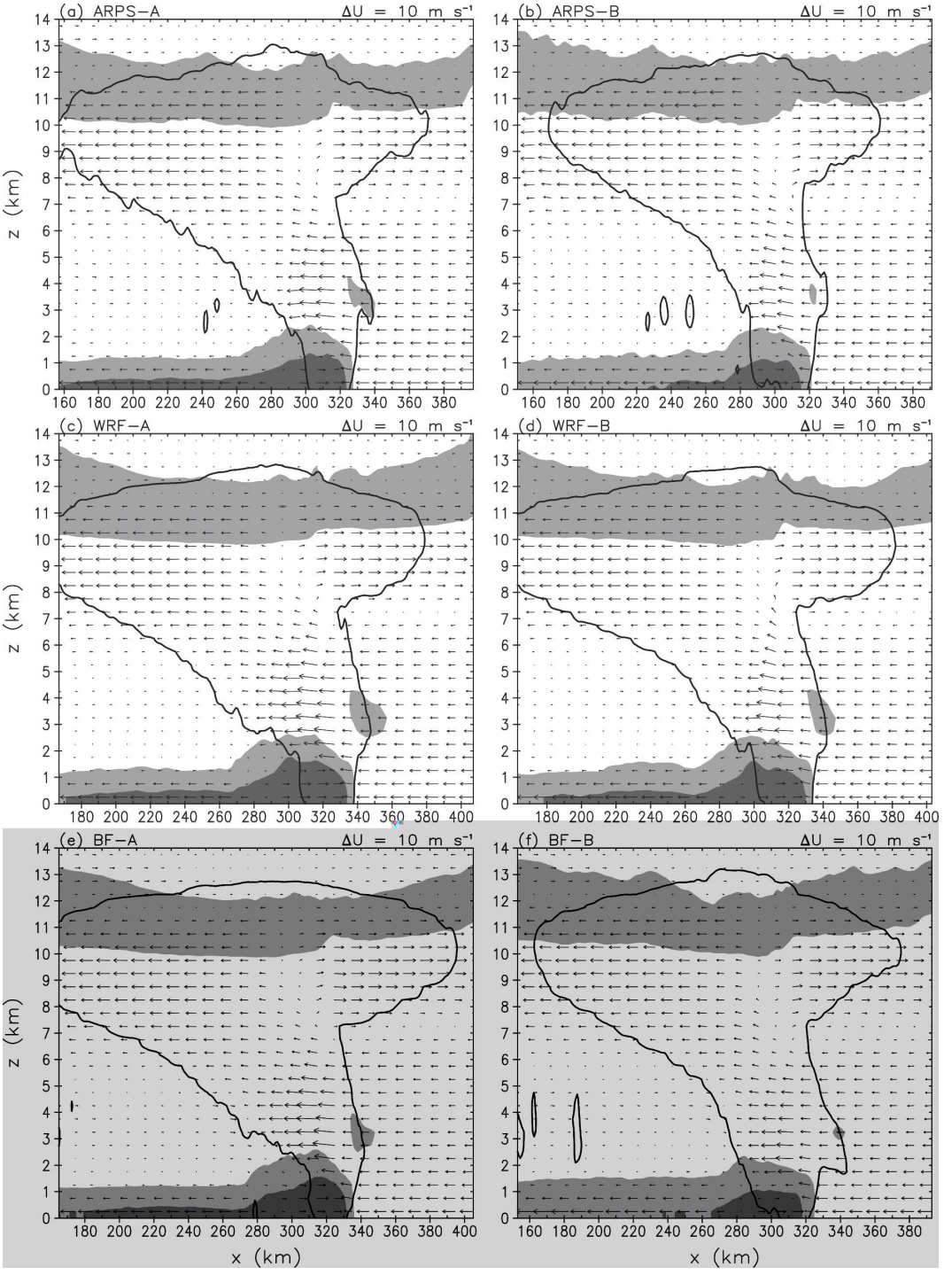

FIG. 2. Line-averaged vertical cross sections at $t = 4$ h for $\Delta U = 10$ m s^{-1} from (a) ARPS-A, (b) ARPS-B, (c) WRF-A, (d) WRF-B, (e) BF-A, and (f) BF-B. System-relative flow vectors are included every 10 km horizontally and every 500 m vertically, with a vector length of 10 km representing a vector magnitude of 15 m s^{-1}. The 1×10^{-2} g kg^{-1} cloud water contour indicates the cloud boundary. Buoyancy is shaded, with light gray representing < -0.01 m s^{-2} and dark gray representing < -0.1 m s^{-2}.

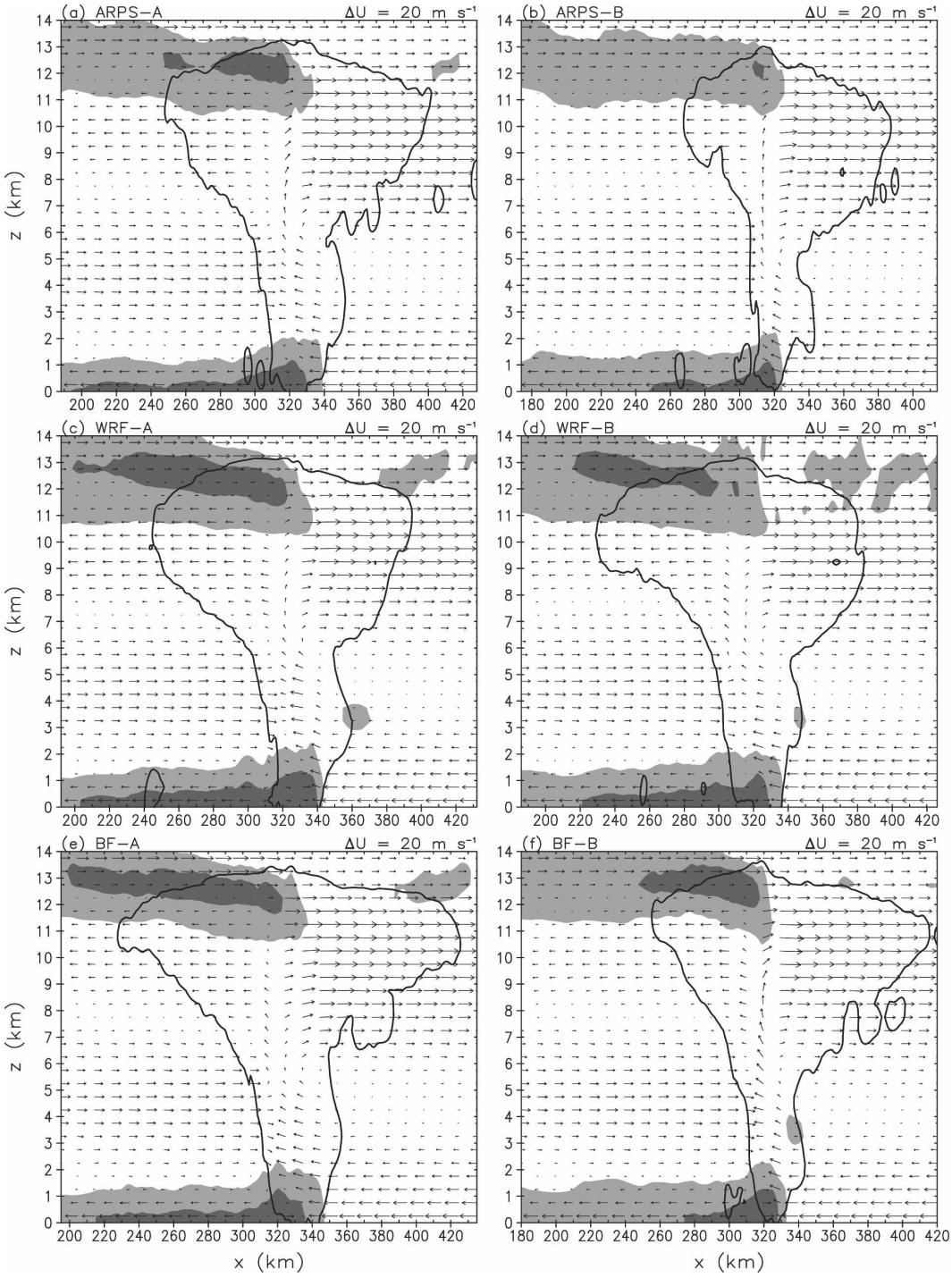

FIG. 3. Same as in Fig. 2, but for $\Delta U = 20\ \mathrm{m\ s^{-1}}$.

weaker cold pools and more slowly developing squall lines. For example, the ARPS-B and BF-B simulations have considerably narrower upper-tropospheric cloud compared with the corresponding -A simulations. This difference can be directly attributed to the enhanced diffusion in the former simulations, which weakens the updrafts, leading to less condensate, less evaporation, and consequently weaker cold pools. These differences are quantified in the next section.

With enhanced diffusion through the subgrid turbu-

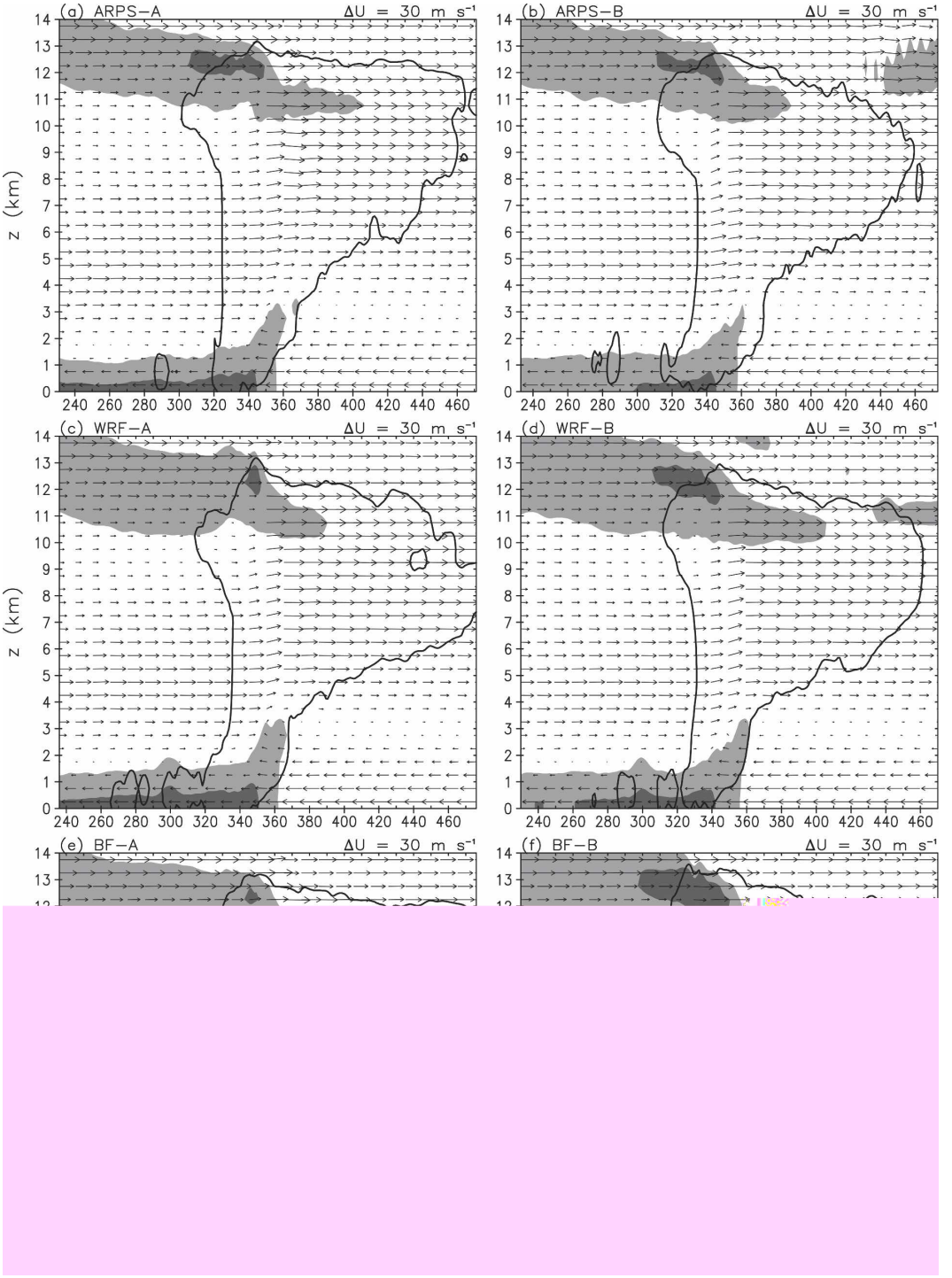

FIG. 4. Same as in Fig. 2, but for $\Delta U = 30$ m s^{-1}.

lence scheme, the WRF-B results are roughly similar to the WRF-A results when $\Delta U = 10$, 20, and 30 m s^{-1} (Figs. 2c,d, 3c,d, and 4c,d), but not in other shears. When $\Delta U = 0$ m s^{-1}, the increase of C_k substantially reduces the number of cells in the convective region (Figs. 5c,d). In addition, as reported in the previous section, the WRF-B configuration does not produce a squall line when $\Delta U = 40$ m s^{-1}.

It is possible that diffusion would have a lesser effect on convective cells if higher resolution were used. The

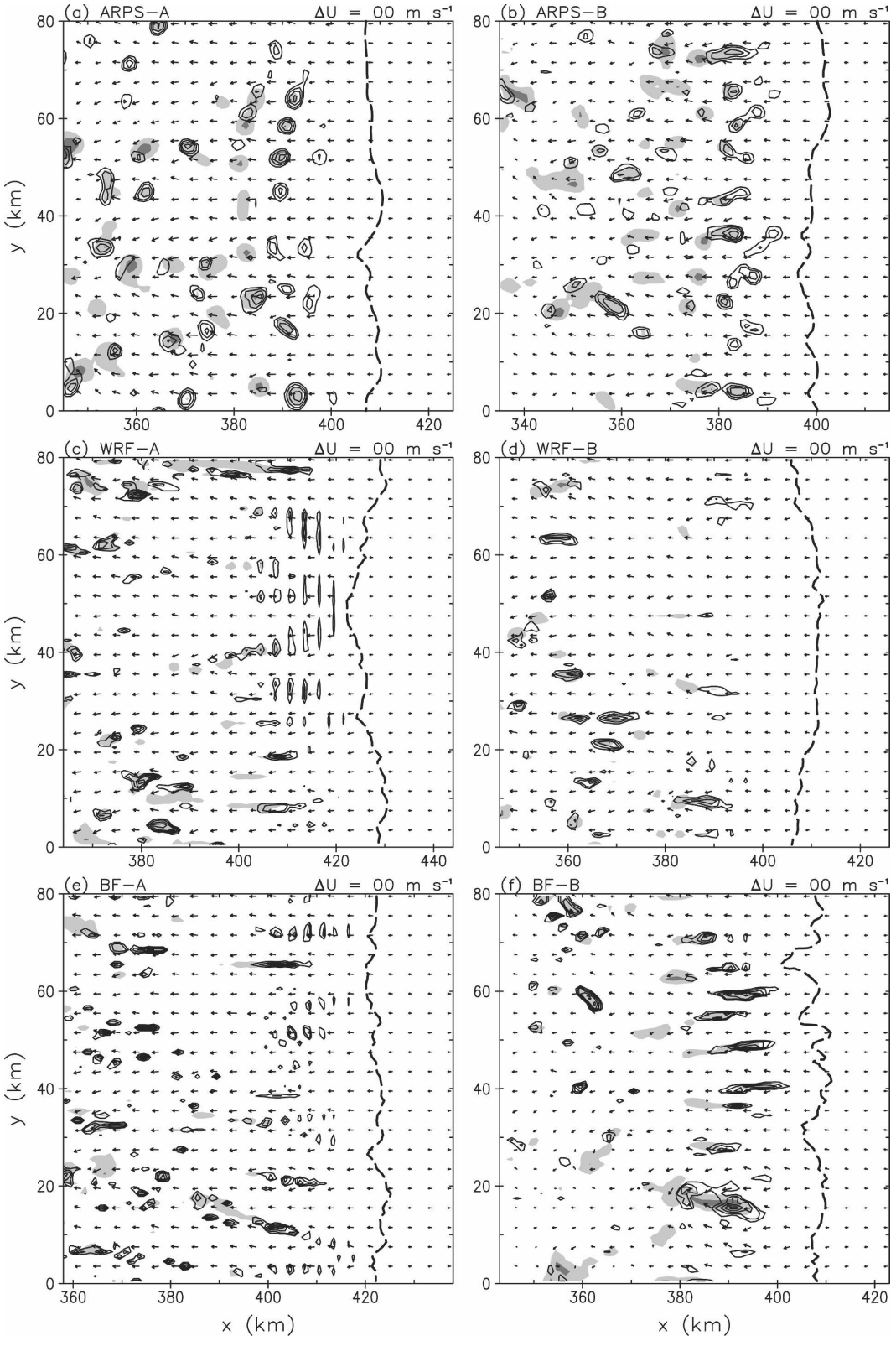

FIG. 5. Horizontal cross sections at $z = 3$ km and $t = 4$ h for $\Delta U = 0$ m s^{-1} from (a) ARPS-A, (b) ARPS-B, (c) WRF-A, (d) WRF-B, (e) BF-A, and (f) BF-B. Positive vertical velocity is contoured every 2 m s^{-1}. Rainwater mixing ratio is shaded, with light gray representing >1 and dark gray representing >4 g kg^{-1}. Line-relative flow vectors are included every 4 km, with a vector length of 4 km indicating a vector magnitude of 20 m s^{-1}. The thick dashed contour is the surface gust front.

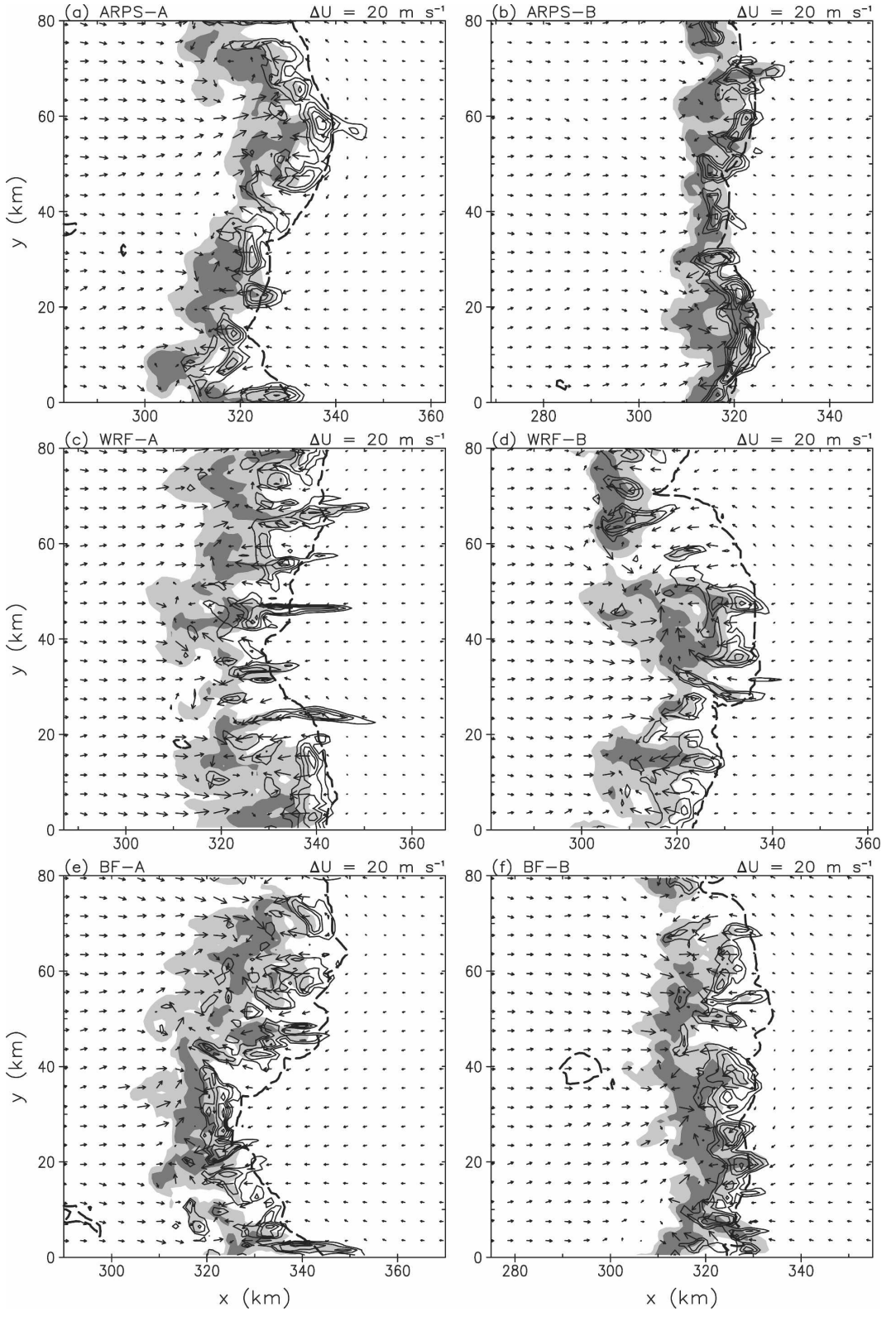

FIG. 6. Same as in Fig. 5, but for $\Delta U = 20$ m s^{-1}. The contour interval for vertical velocity is 3 m s^{-1}.

diffusion schemes in these models act primarily at small scales (less than ~8 times the grid spacing, or 8 km herein). However, in our simulations the updrafts are roughly 4–8 km wide, so diffusion acts directly on them. Future studies should reevaluate the impact of diffusion and model configuration when using higher resolution, so that diffusion does not act on the scale of the convective updrafts.

A second notable difference among models is the tendency for the KW model to produce the deepest and strongest cold pools. When $\Delta U = 10\ \mathrm{m\ s^{-1}}$, the comparable figure from WR04 of line-averaged structure (WR04, their Fig. 12b) shows the $-0.01\ \mathrm{m\ s^{-1}}$ buoyancy value at a height of 2 km at all locations west of the cloud boundary. In contrast, this buoyancy value is below 1.5 km, and typically below even 1.25 km, in all simulations by the newer numerical models (Fig. 2). This tendency of the KW model to produce the strongest and deepest cold pools is probably the most salient result from this model comparison. Further details are provided in later sections of this paper.

A third notable difference is the tendency for some of the weakly diffusive, -A, simulations to be characterized by an artificial updraft pattern (e.g., Figs. 5c,e). Specifically, the cells are often poorly resolved and have a regularly repeating pattern in both the along-line and across-line directions. This pattern is especially prevalent when the low-level shear is weak. This is the same problem studied with an earlier version of the WRF model by Takemi and Rotunno (2003). In a similar study, Bryan (2005) argued that the pattern arises from oscillatory numerics applied to flow through statically unstable layers. Consequently, nonoscillatory numerical schemes and strong diffusion at small scales should be less likely to produce the pattern.

The KW model simulations produce larger updrafts and do not show evidence of an artificial organization (WR04, their Fig. 13b). We attribute this difference in cellular structure to two characteristics of the KW model's diffusion schemes. First, the fourth-order horizontal diffusion in the KW model contributes to the creation of larger cells because of the lower effective resolution allowed by this scheme (Skamarock 2004). The ARPS-A run uses the same diffusion scheme and also produces larger cells than the WRF and BF models produce (e.g., Fig. 5a). The implicit diffusion in the WRF and BF models has a sixth-order form, which permits a higher effective resolution when a comparable diffusion coefficient is used (i.e., when 2Δ features are diffused at the same rate; Skamarock 2004).

A second significant attribute of the KW model configuration is the strong vertical diffusion acting on perturbation fields. In their 2005 corrigendum, Takemi and Rotunno (2003) reported that vertical diffusion acting on total fields in the WRF model was more diffusive and resulted in fewer cells, whereas diffusion acting on perturbation fields generated significantly more cells that were also stronger. This analysis by Takemi and Rotunno (2003) is not directly relevant to the scheme in the KW model because they addressed the formulation of the subgrid turbulence parameterization, not the second-order artificial diffusion term. Nevertheless, their differences in results are significant, and may explain differences among our simulations, especially considering that the KW model is the only configuration we used that applies vertical diffusion on perturbation fields.

A fourth notable difference among models is the tendency for the simulations with higher effective resolution (i.e., the WRF and BF models) to produce elongated, plumelike updrafts in the convective region (e.g., Figs. 5f and 6c). Houze (2004) speculated that such structures may be responsible for "cigar-shaped" radar echoes that are sometimes observed in the convective region of mesoscale convective systems. These features have been studied in detail with high-resolution ($\Delta x = 125$ m) simulations by Bryan et al. (2006); in their simulations, the plumes had an average spacing of ~3 km. Thus, they are poorly resolved with the 1-km grid spacing we used, and this might explain why they seem to be more common with model configurations that have a higher effective resolution.

In summary, there are some minor differences in system structure among the four models' simulations, but the overall qualitative structures are very similar. This conclusion seems to be reached in all model comparison studies of mesoscale convective systems, and also holds for model comparisons that use more realistic physical processes such as ice microphysics, surface fluxes, and radiation (e.g., Redelsperger et al. 2000; Derbyshire et al. 2004).

Furthermore, for all of our model configurations, the trend in system structure with increasing shear is the same as that found by WR04. That is, updraft intensity increases and cells become larger as low- to midlevel environmental shear increases (cf. Figs. 5 and 6). The trend from weak, upshear-tilted systems in weak shear to strong, downshear-tilted systems in strong shear is clearly captured in all simulations (Figs. 2–4). This specific aspect of RKW theory's application to squall lines—that variations in low- to midlevel shear alone can produce a broad range of system structures, all else being equal—is supported by all four numerical models.

4. The optimal state

A more controversial aspect of RKW theory is the argument for an optimal state, wherein the upshear acceleration from the cold pool roughly balances the downshear acceleration from the environmental shear. When approximate balance occurs, the lifting at the leading edge of the system should be the strongest and deepest according to the theory (all else being equal). Undoubtedly, a balance can occur; however, some have questioned whether such balance is relevant to the squall lines' overall characteristics.

WR04 evaluated this optimal state quantitatively via C, a measure of cold pool intensity, and via ΔU, a measure of shear in low to midlevels. Theoretically, the optimal state occurs when the ratio $C/\Delta U$ is approximately 1. One of the outstanding questions concerning RKW theory is the following: what effect does this ratio have on other system properties, such as overall intensity?

WR04 showed that the value of $C/\Delta U$ does conform to the overall system structure predicted by the theory. Upshear-tilted structures dominate when $C/\Delta U > 1$, and downshear-tilted structures dominate when $C/\Delta U < 1$ (cf. Tables 1a and 1c by WR04). Hence, there is rather convincing evidence that the ratio $C/\Delta U$ does have a strong influence on the overall structure of simulated squall lines, at least within the constraints of WR04's study.

However, this result does not directly bear on concerns about the relevance of the optimal state to system intensity. To address these concerns, WR04 presented several quantitative measures of system intensity, such as wind speed at the lowest model level and total rainfall. They noted that systems tended to be more intense when $C/\Delta U$ was close to 1. For example, as shear in low levels was increased, $C/\Delta U$ decreased from ~2 to ~1, and system intensity increased accordingly.

On the other hand, Stensrud et al. (2005) noted that WR04's quantitative measures usually did not peak when $C/\Delta U$ was about 1. In their statistical analysis of all simulations in the WR04 study, Stensrud et al. found that total rainfall peaked at $C/\Delta U = 0.5$, maximum updraft at $C/\Delta U = 0.6$, and average surface wind at $C/\Delta U = 1.8$. Only maximum surface wind had a maximum value when $C/\Delta U \approx 1$.

In this section, we evaluate the relevance of the optimal state to measures of system intensity with our new simulations, using the same techniques used by WR04. We do not assess the methodology of WR04, but rather we assess whether their conclusions are dependent on the numerical model used for such a study.

Theoretically, C is the propagation speed of a two-dimensional density current in an infinitely deep, unstratified environment (Benjamin 1968),

$$C^2 = 2\int_0^H (-B)\, dz, \tag{1}$$

wherein H is the cold pool depth; B is buoyancy,

$$B \equiv g\left[\frac{\theta - \bar{\theta}}{\bar{\theta}} + 0.61(q_v - \bar{q}_v) - q_c - q_r\right]; \tag{2}$$

θ is potential temperature; overbars indicate the model's base state, which in these simulations is the initial condition; and q_v, q_c, and q_r are the mixing ratios of water vapor, cloud water, and rainwater, respectively. We calculate C from the model output in the same manner as WR04 did, except we use hourly output from t = 3 to 6 h.

We define ΔU as the wind change in the lowest 5 km, because this is consistent with WR04. In principle, the appropriate layer to consider would be the depth of the cold pool; in fact, the simulations of idealized density currents by WR04 showed that cold pool lifting was optimized when shear was confined to this layer. However, WR04 (p. 376) provided several arguments for using the 0–5-km layer, instead of the layer matching the cold pool depth. For example, they showed that shear above the cold pool can contribute to cell generation, which has also been shown by Fovell and Dailey (1995) and Fovell and Tan (1998).

Also following the technique of WR04, we neglect the potentially important effect of the rear-inflow jet on the vorticity balance at the leading edge of the system. Weisman (1992) showed how the rear-inflow jet could be quantitatively included in the RKW balance relation. The importance of the rear-inflow jet is discussed in his paper, as well as in the papers by Lafore and Moncrieff (1989) and Fovell and Ogura (1989). However, WR04 (p. 376) excluded this contribution to system structure because the ratio $C/\Delta U$ alone "still provides a useful guide of overall system structure for a wide range of shear environments."

In the overall design of the simulations, ΔU is the only parameter that is varied from one run to the next. Studies using this method often cite the ΔU value that produces the optimal condition ($C/\Delta U = 1$), which we refer to as the *optimal shear* (ΔU_{optim}). We also analyze the ΔU that leads to maxima in certain quantitative values (e.g., rainfall, surface winds), which we refer to as ΔU_{max}. If ΔU_{optim} and ΔU_{max} have similar values, it supports the relevance of RKW theory to squall lines.

Calculations of C confirm the qualitative conclusion from the previous section that the KW model usually produces the deepest, strongest cold pools (Fig. 7a).

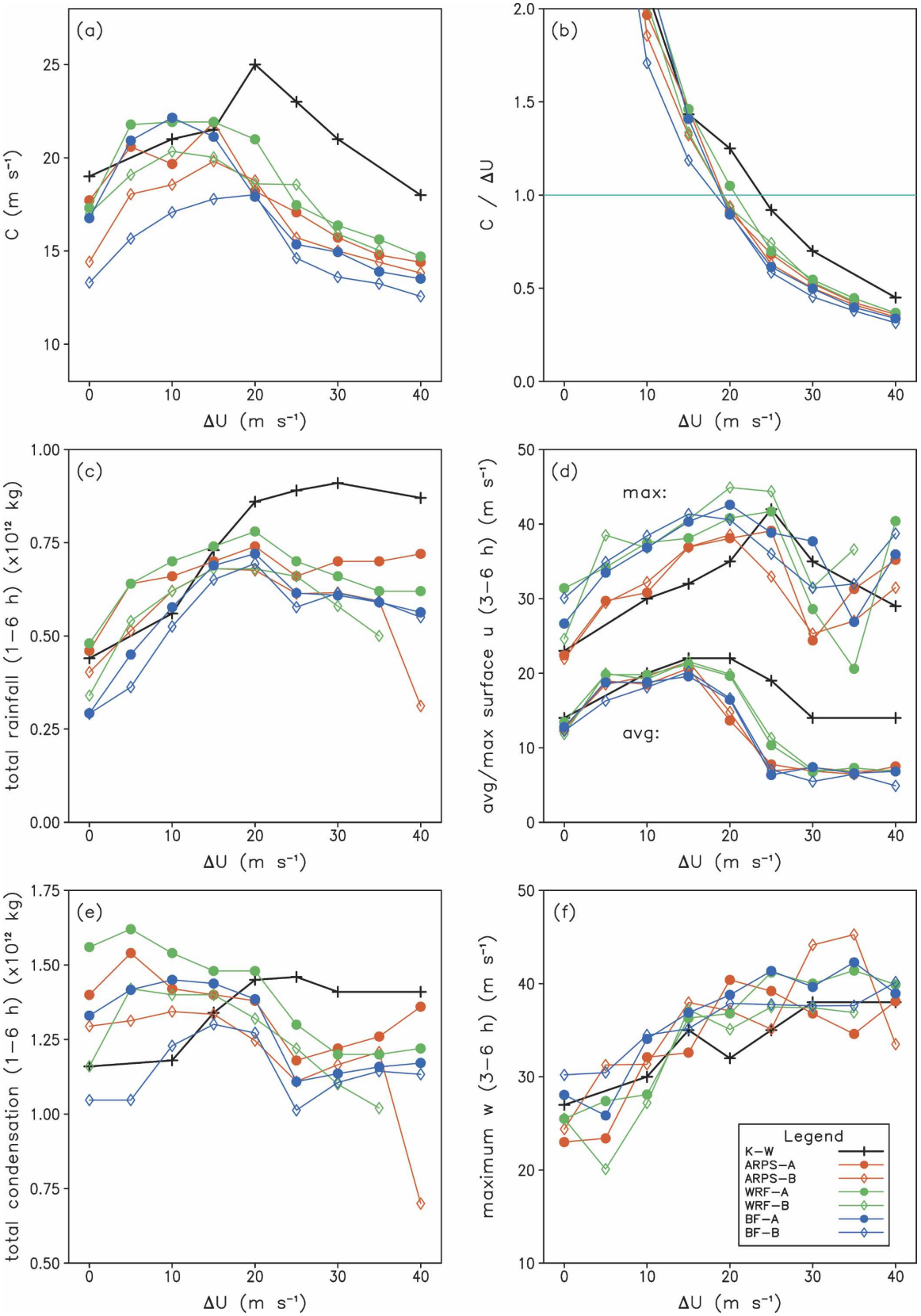

FIG. 7. Quantitative output as a function of ΔU from the seven model configurations: (a) C, (b) $C/\Delta U$, (c) total rainfall, (d) maximum (upper set of curves) and averaged (lower set) west–east winds at the lowest model level, (e) total condensation, and (f) maximum vertical velocity. The cyan horizontal line in (b) denotes $C/\Delta U = 1$. In (c) and (e), the values from the ARPS, WRF, and BF models have been multiplied by 2 to account for the different domain sizes compared to the simulations with the KW model.

TABLE 2. The value of ΔU for which measures of system intensity are maximized (ΔU_{max}).

Model	ΔU_{max}					
	C	Tot rainfall	u_{avg}	u_{max}	Tot condensation	w_{max}
KW	20	30	15 and 20	25	25	30
ARPS-A	15	20	15	25	5	20
ARPS-B	15	15	15	20	10	35
WRF-A	15	20	15	25	5	35
WRF-B	10	15	15	20	5	25
BF-A	10	20	15	20	10	35
BF-B	20	20	15	15	15	40
Avg (excluding KW)	14	18	15	21	8	32

The only exception is in weak shears, for which the KW model results are similar to the −A model configurations. The average ΔU_{max} for C is 14 m s^{-1} with the newer models, but is 20 m s^{-1} with the KW model (Table 2). In fact, there is a sharp increase in C with the KW model between 15 and 20 m s^{-1}; a similar feature does not occur with any other numerical model (Fig. 7a).

More relevant to RKW theory is the ratio $C/\Delta U$. When plotted as a function of ΔU, it is apparent that the KW model produces the optimal state ($C/\Delta U = 1$) at a larger shear than do the other models (Fig. 7b); $\Delta U_{optim} = 24$ m s^{-1} for the KW model, whereas the average ΔU_{optim} for the six other simulations is 19 m s^{-1}, which is 20% lower (Table 3). This is a key finding: the KW model requires a significantly stronger shear to produce the optimal state. This model bias might explain some differences between conclusions based on simulations by the KW model and conclusions based on observational studies of severe convective windstorms [e.g., section 4b(3) of Coniglio et al. 2004a].

For total rainfall, the KW model is again an outlier in stronger shears (Fig. 7c). The KW model produces 20%–50% more rainfall than any other model when $\Delta U > 20$ m s^{-1}. Furthermore, the KW model rainfall peaks at a considerably stronger shear, $\Delta U_{max} = 30$ m s^{-1}, as opposed to an average ΔU_{max} of 18 m s^{-1} for the other models (Table 2).

As WR04 did, we use wind speed at the lowest model level ($z = 250$ m) as a proxy for surface winds. (For the WRF model, wind speeds are interpolated to $z = 250$ m). Also following WR04, we compute average surface winds u_{avg} associated with each squall line, by calculating the average west–east wind speed u at a location 10 km behind the surface gust front (defined as $\theta' = -1$ K). The results (bottom set of curves in Fig. 7d) reveal a tendency for the KW model to produce stronger surface winds, especially in strong shear. All of the newer models agree well with each other, and produce similar results for both the −A and −B configurations. The WRF model appears to have a slight tendency to produce stronger surface winds, but this might be related to the slightly higher vertical resolution near the surface ($\Delta z \approx 475$ m). All of the newer models yield $\Delta U_{max} = 15$ m s^{-1} for this variable, while for the KW model $\Delta U_{max} = 15$ and 20 m s^{-1} (Table 2).

For maximum surface winds at any location and time u_{max}, some models produce a pronounced increase when ΔU increases from 35 to 40 m s^{-1} (Fig. 7d, the upper set of curves). In this highly sheared environment, the simulated cells are supercellular. Technically, RKW theory only applies to quasi-linear convective systems, and not to lines of supercells. Accordingly, considering only the 0–30 m s^{-1} range to exclude these cases, the newer models yield an average ΔU_{max} of 21 m s^{-1} for u_{max}, which is again lower than the result from the KW model ($\Delta U_{max} = 25$ m s^{-1}; Table 2).

Other quantitative measures analyzed by WR04 are more ambiguous in their application to RKW theory's relevance to squall-line intensity. Total condensation has the most scatter of any variable we analyzed, particularly in weak shear (Fig. 7e). For this variable, the KW model produces among the lowest values in weak shear, but the highest values in strong shear. The greatest differences between the KW model and newer models is in ΔU_{max} for total condensation, with $\Delta U_{max} = 25$ m s^{-1} for the former, but an average $\Delta U_{max} = 8$ m s^{-1}

TABLE 3. The value of ΔU for which $C/\Delta U$ is 1 (i.e., the optimal shear, ΔU_{optim}), derived by interpolating from data points in Fig. 7b.

Model	ΔU_{optim} (m s^{-1})
KW	24
ARPS-A	19
ARPS-B	19
WRF-A	21
WRF-B	19
BF-A	19
BF-B	18
Avg (excluding KW)	19

for the latter (Table 2). Thus, in terms of RKW theory, total condensation does not support the optimal-state argument because $\Delta U_{\max}$ for total condensation is far below the optimal shear value (excluding the results from the KW model). We suspect that the variability in weak shears is partly attributable to the spurious updraft pattern discussed in the previous section. On the other hand, it is possible that the inclusion of ice microphysics would change the expected result. Strongly upshear-tilted squall lines typically have large stratiform regions, within which significant condensation can occur, owing to the mesoscale updraft above the melting level (e.g., Smull and Houze 1987); in this context, suboptimal squall lines might be expected to have more total condensation than more upright systems. Nevertheless, this is one of the reasons why several measures of system intensity are included in our analysis, and in the analysis by WR04.

For maximum updraft velocity $w_{\max}$, there is good general agreement between all models (Fig. 7f). In fact, $w_{\max}$ is the only variable we analyzed for which the KW model was not an outlier. The trend in this variable also does not show an intensity peak near the optimal state, because $\Delta U_{\max}$ is much greater than the optimal shear value (Table 2). Presumably, this tendency for maximum updraft to increase with stronger shear is related to dynamical effects of updrafts in shear, as discussed by WR04.

Our broad determination is that the newer models support WR04's conclusions more than the KW model does. That is, some measures of overall system intensity *are* greatest when the systems are approximately upright. Furthermore, this upright structure occurs when $C/\Delta U \approx 1$ (i.e., when the cold pool intensity approximately balances the magnitude of environmental shear). This supports WR04's contention that $C/\Delta U$ has an influence on overall system intensity.

In contrast, the squall lines simulated with the KW model switch from predominantly upshear to downshear tilted at a significantly stronger shear (>20 m s^{-1} based on WR04's Fig. 12, as opposed to <20 m s^{-1} in the case of the other models, based on Figs. 2–3 herein). However, peak values of overall system intensity from the KW model simulations are not consistent with the value of ΔU_{optim}, as indicated in Table 2.

Thus, there is convincing evidence here that some of the criticisms of RKW theory's applicability to squall lines (e.g., Stensrud et al. 2005) are attributable to the numerical model used by RKW88 and WR04, but not necessarily to the theory itself. The results from newer, more accurate models with higher effective resolution show better consistency between theory and results than the KW model used by RKW88 and WR04.

This result should not be interpreted as definitive support for RKW theory's relevance to squall-line structure and intensity. We have not addressed the concern that changes in squall-line characteristics might be more attributable to ΔU than to $C/\Delta U$ (e.g., Stensrud et al. 2005). This ambiguity is a consequence of the experimental design, in which ΔU is the only parameter that varies. To address this concern, future studies could hold shear fixed while systematically changing parameters that affect C (like midlevel equivalent potential temperature). All we can say, at this time, is that the newer numerical models provide *better* support for the arguments of WKR88 and WR04, at least when applied within those authors' constraints. Future studies could also explore possible effects of ice microphysics, higher resolution, and variations in upper-level shear. It is possible that systems should not be expected to have a peak intensity when $C/\Delta U \approx 1$, especially given the lack of extensive stratiform regions in the absence of ice microphysics, and owing to the omission of the rear-inflow jet in our assessment of the optimal condition (e.g., Fovell and Ogura 1989; Weisman 1992). We return to these points in the conclusions section of this paper.

5. Systematic model differences

For idealized simulations such as these, there is no "truth" solution to compare against. However, by comparing results from the four models, we have identified notable differences that, in some cases, have illuminated errors in model code. (These errors were corrected for all simulations presented herein.) A similar conclusion on the utility of model comparisons was drawn by Redelsperger et al. (2000). In this section, we explore in detail some of the more notable systematic differences. Our goal is to identify a root cause of each difference, and thereby to provide guidance to model developers and users.

a. The BF model's moisture

Although the difference is rather subtle, we find that the BF model tends to produce the lowest quantitative water budget measures (total rainfall, total rainwater evaporation, etc.). The BF model is the only model of the four that accounts for the specific heats of water in its governing equations. This effect usually produces 10%–20% *more* condensation and rainfall in simulations that use traditional cloud model equations (Bryan and Fritsch 2002). Thus, the BF model's tendency to produce the least rainfall (Fig. 7c) is unexpected.

We attribute this difference to improved total water

conservation in the BF model compared to most of the other model configurations. For the BF-A configuration, the model uses an oscillatory advection scheme. Such schemes produce spurious "undershoots" that can result in negative water mass. Often, numerical models used to simulate severe convective storms simply set negative water values to zero, without moving water from elsewhere in the domain to conserve total water. This technique, hereafter referred to as the nonconserving technique, acts as an artificial source of water. Some studies have investigated the quantitative effects of the nonconserving technique (e.g., Xue et al. 2001, p. 154), but many model developers consider this artificial increase in mass to be minor.

There are several methods to remedy this unphysical situation, including, but not necessarily limited to, the following: using a nonoscillatory advection scheme (e.g., Smolarkiewicz and Grabowski 1990; Xue et al. 2001); implementing a flux limiter to the advection of moisture to prevent the creation of negative values by advection (e.g., Lafore et al. 1998; Xue et al. 2001); predicting a transformed mass variable that minimizes the impact of the underprediction (e.g., Ooyama 2001); or applying schemes that borrow water from other parts of the domain to preserve total mass when filling in negative values (e.g., Cohen 2000).

For our simulations, the BF model sets negative water values to zero by moving water of the same class from neighboring grid points. The technique is nearly the same as that described by Cohen (2000), and is referred to herein as the forced-conservation technique. The BF-B configuration uses a nonoscillatory advection scheme for moisture, which does not require the forced-conservation technique. Tests with the BF model show that simulations using the nonconserving technique can have >25% more condensate in the domain than simulations that use the forced-conservation technique.

With one exception, our configurations of the KW, ARPS, and WRF models use the nonconserving technique. This exception is the ARPS-B configuration, which uses a nonoscillatory advection scheme for moisture, and conserves water well. In fact, the ARPS-B has less rainfall and condensation, on average, than any model except the BF model. It should be noted that the WRF model's dynamical core conserves total water, but its Kessler microphysics code sets negative water values to zero.

Overall, we conclude that the water-conserving model configurations that we used produce systematically less rainfall compared to the nonconserving configurations (e.g., Fig. 7c). For the nonconserving configurations, the artificially increased condensate ultimately leads to more rainwater, more evaporation, and stronger cold pools. In support of this interpretation, the full suite of simulations was produced using the BF model but without the forced-conservation technique (hereafter referred to as BF-C). These simulations had up to 20% larger values of C (Fig. 8a), owing to greater evaporation. The C values from BF-C are nearly the same as those from WRF-A, suggesting that the differences between WRF-A and BF-A are largely attributable to improved water conservation in the BF model. Compared to the BF-A runs, total rainfall from BF-C is 85% larger when $\Delta U = 0$ m s^{-1}, decreasing to 20%

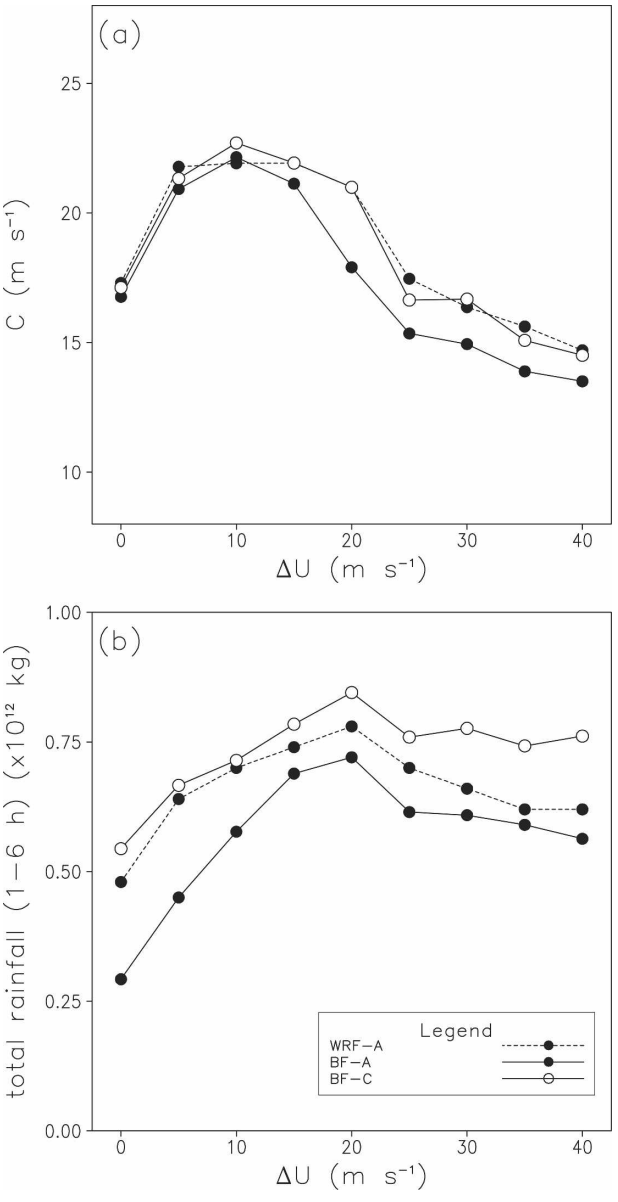

FIG. 8. Quantitative output from simulations with WRF-A, BF-A, and BF-C: (a) C and (b) total rainfall.

larger in stronger shears (Fig. 8b). Rainfall from BF-C is greater than that from WRF-A, possibly owing to the different thermodynamical equations in the models. In general terms, these results are not necessarily surprising; however, the error in total water is larger than we expected. This highlights the need to conserve water if quantitative precipitation values are important to model users.

On the other hand, as it pertains to the main focus of this paper, water conservation has essentially no effect on the assessment of RKW theory. When measures of system intensity are compared to $C/\Delta U$, the results from BF-C yield the same answers as those from BF-A. Hence, some model configurations, even though they are unphysical, have no impact on the assessment of RKW theory's relevance to squall lines, at least for this modeling methodology.

b. The KW model's cold pools

The most conspicuous systematic difference we find among the seven model configurations is the tendency for the KW model to produce deeper and more intense surface-based cold pools, especially in stronger shears (e.g., Fig. 7a). After considering several possibilities, we find that the formulation of the artificial vertical diffusion scheme in the KW model is primarily responsible.

In the KW model, artificial vertical diffusion is not applied at the grid points closest to the bottom and top boundaries. This is equivalent to setting the flux at the surface equal to the flux at the nearest grid point inside the domain. Thus, the KW model can have nonzero fluxes at the top and bottom boundaries. Richardson (1999) reached the same conclusion about the vertical diffusion scheme in a comparison between the KW and ARPS models. All other model configurations that we tested have a zero-flux boundary condition at the top and bottom (in the absence of a specified heat flux or surface drag term, which we did not include).

In the KW model, the effective boundary flux at the surface F_{sfc} is

$$F_{\text{sfc}} = -K \left. \frac{\partial \alpha'}{\partial z} \right|_{k=1}, \tag{3}$$

wherein K is the diffusion coefficient, α is the variable being diffused, the prime indicates the deviation from the model's base state, and "$k = 1$" refers to the first w-level inside the domain (top or bottom) for the staggered vertical grid. We focus attention at the bottom boundary for the remaining analysis, because this is where the cold pool resides.

In the environment ahead of and far behind the squall line, conditions near the surface remain approximately the same as in the initial state; in these locations, $\alpha' \cong 0$ and thus $F_{\text{sfc}} \cong 0$. However, in the cold pool, the potential temperature perturbation θ' is negative at the lowest model level and approaches zero with height. Hence, $\partial\theta'/\partial z > 0$ and $F_{\text{sfc}} < 0$ for θ'. For q_v, the perturbation is usually negative in the cold pool at the surface and decreases (i.e., becomes more negative) with height, resulting in a positive flux at the lower boundary. Thus, the cold pool experiences a net cooling (negative flux) and net moistening (positive flux) from the vertical diffusion scheme, compared to schemes that set the flux at the boundaries to zero. In terms of equivalent potential temperature θ_e, the cooling and moistening can offset each other, resulting in approximate θ_e conservation; for example, at 1000 hPa, θ_e will be conserved with cooling of 1 K and moistening of 0.4 g kg^{-1}. The same boundary condition acts on horizontal winds and often increases surface winds in the cold pool.

These surface fluxes from the KW vertical diffusion scheme do not represent a surface heat flux or drag term. Rather, these effective fluxes are artifacts of the artificial diffusion term and the specific boundary condition for this term in the KW model. By eliminating the vertical diffusion at the lowest model level, this implementation ensures that mean profiles cannot be modified by diffusion over time (e.g., Durran and Klemp 1983, p. 2344). This boundary condition is also consistent with the assumption of a free-slip lower boundary. Nevertheless, as formulated, the KW vertical diffusion scheme can act as a source of mass (through θ and q_v) and momentum (through u and v).

Moreover, we believe this formulation of the vertical diffusion term in the KW model is largely responsible for its outlying behavior. To evaluate this hypothesis, we ran a set of BF model simulations with the KW vertical diffusion scheme applied to θ' and without the forced-conservation technique (BF-D), thus making the model more like the KW model. The results strongly support our interpretation. The KW model vertical diffusion scheme clearly increases a cold pool's intensity (Fig. 9a), primarily by increasing its depth. Compared to the original BF-A configuration, the BF-D runs yield similar C values in weak shears, but systematically larger C values in strong shears, much like the results from the KW model (Fig. 9a). In addition, the value of ΔU_{optim} from BF-D is 23 m s^{-1}, which is also similar to the value from the KW model (24 m s^{-1}). Furthermore, with BF-D, total rainfall increases even when $\Delta U > \Delta U_{\text{optim}}$, similar to the trend from the KW model (Fig. 9b).

These results suggest that the vertical diffusion scheme is probably responsible for the different physi-

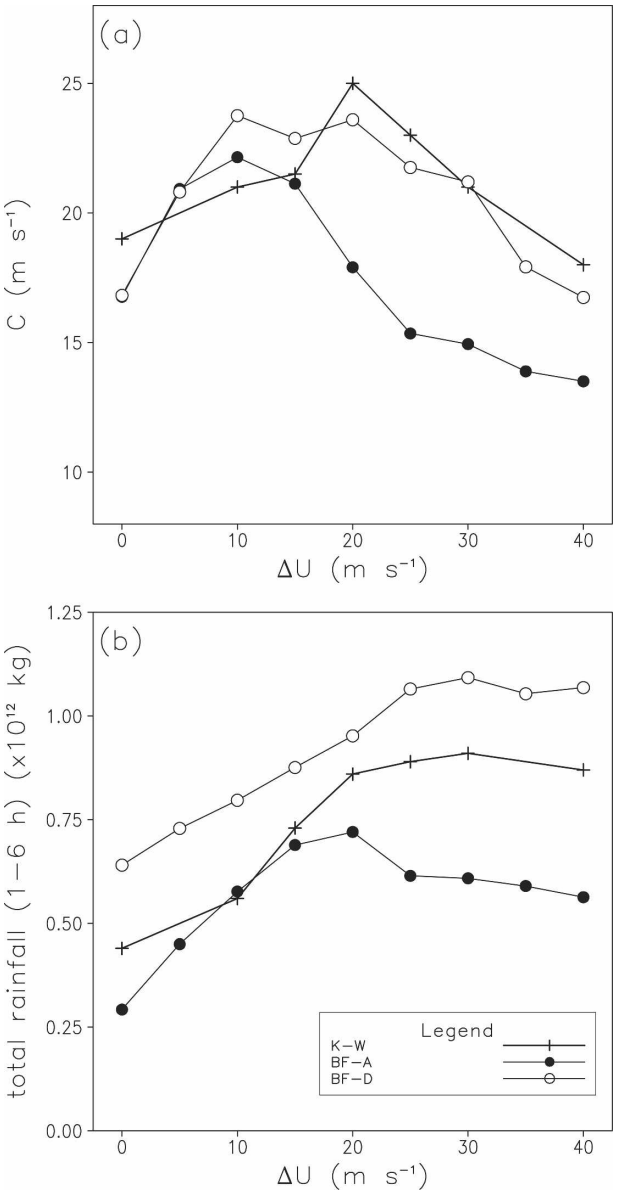

FIG. 9. Quantitative output from simulations with KW, BF-A, and BF-D: (a) C and (b) total rainfall.

cal response in the KW model when $C/\Delta U$ is less than 1. Regardless of the reason, evidence points to a different numerical configuration in the KW model, and corresponding anomalous behavior compared with the other models.

6. Conclusions

a. Summary

Several noteworthy results have emerged from this model comparison. First, we find model comparisons such as this to be useful for illuminating significant differences in model configurations. In some cases, the differences have pointed our attention to coding errors that were not obvious before this study. In contrast to the common practice of using one type of simulation, we recommend that model comparisons should explore a broad physical parameter space, such as environmental shear or thermodynamics. Some differences among the four models in this study were only apparent when results were viewed as a function of shear. For example, anomalous characteristics in the KW model's cold pool and rainfall are not apparent in weak shears, but become obvious when a broad range of shears are simulated.

Second, for these idealized simulations, we see general support for the relevance of RKW theory to squall lines. In terms of system structure, all models lead us to the same qualitative conclusion about changes in shear, with all else being held constant: simulated squall lines have smaller, weaker cells and are tilted upshear in weak 0–5-km shear (with $C/\Delta U > 1$), and have larger, stronger cells and are tilted downshear in strong 0–5-km shear (with $C/\Delta U < 1$). Systems are upright and approximately symmetric at upper levels when $C/\Delta U \approx 1$.

Third, our simulations support the argument that system intensity peaks near the optimal state, at least according to some variables, such as rainfall and near-surface winds. For our experimental design, only ΔU was varied, and the optimal state occurs when ΔU is slightly less than 20 m s^{-1} for all models except for the KW model. More importantly, this is also the approximate shear value that maximizes total rainfall and maximum surface winds for all models except for the KW model. Thus, system intensity is strongest by some measures when $C/\Delta U \approx 1$.

Finally, we diagnosed some systematic model differences uncovered during our study. Most significantly, the KW model produces the deepest and strongest cold pools, likely owing to the way vertical diffusion is formulated near the lower boundary, which provides a source of cooling and moistening in the simulated cold pool. Other model differences, such as artificial updraft patterns and water conservation, have no perceptible impact on the assessment of RKW theory.

b. Discussion

In this paper, we addressed some concerns about RKW theory, such as the relevance of the optimal state to the intensity of simulated squall lines. We found that this latter concern is partially attributable to the KW model used by WR04, but is not necessarily a shortcoming of the theory itself. However, our study does not address all concerns expressed in the literature

about RKW theory, and should not be interpreted as definitive validation of RKW theory's relevance to squall lines.

For example, one concern about RKW theory is its applicability in broader environmental conditions. The simulations of RKW88, WKR88, WR04, and our simulations used only one thermodynamical profile, and therefore they yield a fairly narrow range of C at the squall lines' mature state. The simulations of Weisman (1992, 1993) explored a broader range of thermodynamical conditions (e.g., CAPE from 1000 to 4500 J kg^{-1}), but with a smaller domain and coarser resolution. In principle, RKW theory should be applicable in a wide range of environments because the ratio $C/\Delta U$ is important, not the values of C or ΔU by themselves.

In addition, several recent studies have highlighted how system structure and intensity can depend on shear above the cold pool (e.g., Fovell and Dailey 1995; Parker and Johnson 2004a; Coniglio et al. 2004b). A similar conclusion was reached in analytical and numerical studies of density currents in channels by Xu et al. (1996), Xue et al. (1997), and Xue (2000a, 2002). WR04 addressed this concern by exploring deeper shear profiles and elevated shear profiles in their simulations of nonsteady cold pools and squall lines. Nevertheless, the relative importance of shear at low levels versus upper levels in determining squall-line intensity remains an active area of research.

Future studies could also test the impacts of other model configurations, including the effects of ice microphysics, radiation, and higher resolution. Of particular importance, several studies have shown that ice microphysics are required to produce realistic circulations in simulated convective systems (e.g., Fovell and Ogura 1988; Lafore and Moncrieff 1989; Yang and Houze 1995; Parker and Johnson 2004b,c). The Kessler scheme—used herein and in the simulations of RKW88, WKR88, and WR04—specifies only liquid drops, which have a large fall velocity (>5 m s^{-1}). Consequently, all hydrometeors fall close to the convective line, thereby preventing the formation of extensive stratiform regions. This may be more problematic in strong shears, because the hydrometeors fall ahead of the cold pool and interfere with system inflow (Parker and Johnson 2004c). There seems to be no systematic evaluation of RKW theory in simulations of squall lines with extensive stratiform regions, and this is an obvious avenue for research in the near future.

We have followed the techniques of WR04 in our assessment of squall-line properties, mainly because we wanted to investigate whether the conclusions from such a study depend on the numerical model that is used for the simulations. However, it would be valuable for future studies to evaluate more rigorously the RKW theory. As a specific example, a future study could evaluate the relative role played by the rear-inflow jet, which was identified as an important component of system structure and evolution by Fovell and Ogura (1989), Lafore and Moncrieff (1989), and Weisman (1992), but which WR04 and our study neglected.

Acknowledgments. We thank Morris Weisman and Richard Rotunno for their advice and insight during this project; Stan Trier, Ming Xue, and Robert Fovell for their reviews; and Yvette Richardson for sharing her comparison of simulations using the Klemp–Wilhelmson and ARPS Models. G. Bryan was supported by the Advanced Study Program at NCAR, and M. Parker was supported by the NSF under Grant ATM-0349069. The Mesoscale and Microscale Meteorology Division of NCAR provides the version of the WRF model used herein, and the Center for Analysis and Prediction of Storms at the University of Oklahoma provides the ARPS model. M. Parker began this study when he was a faculty member at the University of Nebraska–Lincoln; the ARPS simulations were performed using the Research Computing Facility at UNL. All figures were created with the Grid Analysis and Display System (GrADS).

REFERENCES

Arakawa, A., and V. R. Lamb, 1977: Computational design of the basic dynamical processes of the UCLA general circulation model. *Methods Comput. Phys.,* **17,** 173–265.

Benjamin, T. B., 1968: Gravity currents and related phenomenon. *J. Fluid Mech.,* **31,** 209–248.

Bryan, G. H., 2005: Spurious convective organization in simulated squall lines owing to moist absolutely unstable layers. *Mon. Wea. Rev.,* **133,** 1978–1997.

——, and J. M. Fritsch, 2002: A benchmark simulation for moist nonhydrostatic numerical models. *Mon. Wea. Rev.,* **130,** 2917–2928.

——, R. Rotunno, and J. M. Fritsch, 2006: Roll circulations in the convective region of a simulated squall line. *J. Atmos. Sci.,* in press.

Cohen, C., 2000: A quantitative investigation of entrainment and detrainment in numerically simulated cumulonimbus clouds. *J. Atmos. Sci.,* **57,** 1657–1674.

Coniglio, M. C., and D. J. Stensrud, 2001: Simulation of a progressive derecho using composite initial conditions. *Mon. Wea. Rev.,* **129,** 1593–1616.

——, ——, and M. B. Richman, 2004a: An observational study of derecho-producing convective systems. *Wea. Forecasting,* **19,** 320–337.

——, ——, and L. J. Wicker, 2004b: How upper-level shear can promote organized convective systems. Preprints, *22d Conf. on Severe Local Storms,* Hyannis, MA, Amer. Meteor. Soc., CD-ROM, 10.5.

Deardorff, J. W., 1980: Stratocumulus-capped mixed layer derived

from a three-dimensional model. *Bound.-Layer Meteor.,* **18,** 495–527.

Derbyshire, S. H., I. Beau, P. Bechtold, J.-Y. Grandpeix, J.-M. Piriou, J.-L. Redelsperger, and P. M. M. Soares, 2004: Sensitivity of moist convection to environmental humidity. *Quart. J. Roy. Meteor. Soc.,* **130,** 3055–3079.

Durran, D. R., and J. B. Klemp, 1983: A compressible model for the simulation of moist mountain waves. *Mon. Wea. Rev.,* **111,** 2341–2361.

Fovell, R. G., and Y. Ogura, 1988: Numerical simulation of a midlatitude squall line in two dimensions. *J. Atmos. Sci.,* **45,** 3846–3879.

——, and ——, 1989: Effect of vertical wind shear on numerically simulated multicell storm structure. *J. Atmos. Sci.,* **46,** 3144–3176.

——, and P. S. Dailey, 1995: The temporal behavior of numerically simulated multicell-type storms. Part I: Modes of behavior. *J. Atmos. Sci.,* **52,** 2073–2095.

——, and P.-H. Tan, 1998: The temporal behavior of numerically simulated multicell-type storms. Part II: The convective cell life cycle and cell regeneration. *Mon. Wea. Rev.,* **126,** 551–577.

Hane, C. E., 1973: The squall line thunderstorm: Numerical experimentation. *J. Atmos. Sci.,* **30,** 1672–1690.

Houze, R. A., Jr., 2004: Mesoscale convective systems. *Rev. Geophys.,* **42,** RG4003, doi:10.1029/2004RG000150.

James, R. P., J. M. Fritsch, and P. M. Markowski, 2005: Environmental distinctions between cellular and slabular convective lines. *Mon. Wea. Rev.,* **133,** 2669–2691.

Kessler, E., 1969: *On the Distribution and Continuity of Water Substance in Atmospheric Circulation. Meteor. Monogr.,* No. 32, Amer. Meteor. Soc., 84 pp.

Klemp, J. B., and R. B. Wilhelmson, 1978: The simulation of three-dimensional convective storm dynamics. *J. Atmos. Sci.,* **35,** 1070–1096.

Lafore, J.-P., and M. W. Moncrieff, 1989: A numerical investigation of the organization and interaction of the convective and stratiform regions of tropical squall lines. *J. Atmos. Sci.,* **46,** 521–544.

——, and Coauthors, 1998: The Meso-NH atmospheric simulation system. Part I: Adiabatic formulation and control simulations. *Ann. Geophys.,* **16,** 90–109.

Moncrieff, M. W., S. K. Krueger, D. Gregory, J.-L. Redelsperger, and W.-K. Tao, 1997: GEWEX Cloud System Study (GCSS) Working Group 4: Precipitating convective cloud systems. *Bull. Amer. Meteor. Soc.,* **78,** 831–845.

Nicholls, M. E., R. H. Johnson, and W. R. Cotton, 1988: The sensitivity of two-dimensional simulations of tropical squall lines to environmental profiles. *J. Atmos. Sci.,* **45,** 3625–3649.

Ooyama, K. V., 2001: A dynamic and thermodynamic foundation for modeling the moist atmosphere with parameterized microphysics. *J. Atmos. Sci.,* **58,** 2073–2102.

Parker, M. D., and R. H. Johnson, 2004a: Structures and dynamics of quasi-2D mesoscale convective systems. *J. Atmos. Sci.,* **61,** 545–567.

——, and ——, 2004b: Simulated convective lines with leading precipitation. Part I: Governing dynamics. *J. Atmos. Sci.,* **61,** 1637–1655.

——, and ——, 2004c: Simulated convective lines with leading precipitation. Part II: Evolution and maintenance. *J. Atmos. Sci.,* **61,** 1656–1673.

Redelsperger, J.-L., and Coauthors, 2000: A GCSS model intercomparison for a tropical squall line observed during TOGA-COARE. I: Cloud-resolving models. *Quart. J. Roy. Meteor. Soc.,* **126,** 823–863.

Richardson, Y., 1999: The influence of horizontal variations in vertical shear and low-level moisture on numerically simulated convective storms. Ph.D. dissertation, University of Oklahoma, 236 pp. [Available from School of Meteorology, University of Oklahoma, 100 E. Boyd, Norman, OK 73019.]

Robe, F. R., and K. A. Emanuel, 2001: The effect of vertical wind shear on radiative–convective equilibrium states. *J. Atmos. Sci.,* **58,** 1427–1445.

Rotunno, R., J. B. Klemp, and M. L. Weisman, 1988: A theory for strong, long-lived squall lines. *J. Atmos. Sci.,* **45,** 463–485.

——, ——, and ——, 1990: Comments on "A numerical investigation of the organization and interaction of the convective and stratiform regions of tropical squall lines." *J. Atmos. Sci.,* **47,** 1031–1033.

Shu, C.-W., 2001: High order finite difference and finite volume WENO schemes and discontinuous Galerkin methods for CFD. ICASE Rep. 2001-11, 16 pp. [Available from NASA Langley Research Center, Hampton, VA 23681-2199.]

Skamarock, W. C., 2004: Evaluating mesoscale NWP models using kinetic energy spectra. *Mon. Wea. Rev.,* **132,** 3019–3032.

——, and J. B. Klemp, 1994: Efficiency and accuracy of the Klemp-Wilhelmson time-splitting technique. *Mon. Wea. Rev.,* **122,** 2623–2630.

——, ——, J. Dudhia, D. O. Gill, D. M. Barker, W. Wang, and J. G. Powers, 2005: A description of the Advanced Research WRF version 2. NCAR Tech. Note NCAR/TN-468+STR, 88 pp.

Smolarkiewicz, P. K., and W. W. Grabowski, 1990: The multidimensional positive definite advection transport algorithm: Nonoscillatory option. *J. Comput. Phys.,* **86,** 355–375.

Smull, B. F., and R. A. Houze Jr., 1987: Dual-Doppler radar analysis of a midlatitude squall line with a trailing region of stratiform rain. *J. Atmos. Sci.,* **44,** 2128–2148.

Stensrud, D. J., M. C. Coniglio, R. P. Davies-Jones, and J. S. Evans, 2005: Comments on " 'A theory for strong long-lived squall lines' revisited." *J. Atmos. Sci.,* **62,** 2989–2996.

Szeto, K. K., and H.-R. Cho, 1994: A numerical investigation of squall lines. Part II: The mechanics of evolution. *J. Atmos. Sci.,* **51,** 425–433.

Takemi, T., and R. Rotunno, 2003: The effects of subgrid model mixing and numerical filtering in simulations of mesoscale cloud systems. *Mon. Wea. Rev.,* **131,** 2085–2101; Corrigendum, **133,** 339–341.

Thorpe, A. J., M. J. Miller, and M. W. Moncrieff, 1982: Two-dimensional convection in non-constant shear: A model of midlatitude squall lines. *Quart. J. Roy. Meteor. Soc.,* **108,** 739–762.

Weisman, M. L., 1992: The role of convectively generated rear-inflow jets in the evolution of long-lived mesoconvective systems. *J. Atmos. Sci.,* **49,** 1826–1847.

——, 1993: The genesis of severe, long-lived bow echoes. *J. Atmos. Sci.,* **50,** 645–670.

——, and R. Rotunno, 2004: "A theory for strong long-lived squall lines" revisited. *J. Atmos. Sci.,* **61,** 361–382.

——, J. B. Klemp, and R. Rotunno, 1988: Structure and evolution of numerically simulated squall lines. *J. Atmos. Sci.,* **45,** 1990–2013.

Wicker, L. J., and W. C. Skamarock, 2002: Time splitting methods for elastic models using forward time schemes. *Mon. Wea. Rev.,* **130,** 2088–2097.

Wilhelmson, R. B., and C. S. Chen, 1982: A simulation of the development of successive cells along a cold outflow boundary. *J. Atmos. Sci.,* **39,** 1466–1483.

Xu, K.-M., and Coauthors, 2002: An intercomparison of cloud-resolving models with the Atmospheric Radiation Measurement summer 1997 Intensive Observation Period data. *Quart. J. Roy. Meteor. Soc.,* **128,** 593–624.

Xu, Q., M. Xue, and K. K. Droegemeier, 1996: Numerical simulations of density currents in shear environments within a vertically confined channel. *J. Atmos. Sci.,* **53,** 770–786.

Xue, M., 2000a: Density currents in two-layer shear flows. *Quart. J. Roy. Meteor. Soc.,* **126,** 1301–1320.

——, 2000b: High-order monotonic numerical diffusion and smoothing. *Mon. Wea. Rev.,* **128,** 2853–2864.

——, 2002: Density currents in shear flows: Effects of rigid lid and cold-pool internal circulation, and application to squall line dynamics. *Quart. J. Roy. Meteor. Soc.,* **128,** 47–73.

——, Q. Xu, and K. K. Droegemeier, 1997: A theoretical and numerical study of density currents in nonconstant shear flows. *J. Atmos. Sci.,* **54,** 1998–2019.

——, K. K. Droegemeier, and V. Wong, 2000: The Advanced Regional Prediction System (ARPS)—A multiscale nonhydrostatic atmospheric simulation and prediction model. Part I: Model dynamics and verification. *Meteor. Atmos. Phys.,* **75,** 161–193.

——, and Coauthors, 2001: The Advanced Regional Prediction System (ARPS)—A multiscale nonhydrostatic atmospheric simulation and prediction model. Part II: Model physics and applications. *Meteor. Atmos. Phys.,* **76,** 143–165.

Yang, M.-J., and R. A. Houze Jr., 1995: Sensitivity of squall-line rear inflow to ice microphysics and environmental humidity. *Mon. Wea. Rev.,* **123,** 3175–3193.

Zalesak, S. T., 1979: Fully multidimensional flux-corrected transport algorithms for fluids. *J. Comput. Phys.,* **31,** 335–362.